JOURNAL OF MATERIALS SCIENCE 25 (1990) 697–705

A unified model of stress relaxation and creep applied to oriented polyethylene

J. SWEENEY, I .M. WARD
Department of Physics, University of Leeds, Leeds LS2 9JT, UK

The stress relaxation behaviour of high-modulus oriented polyethylene fibre has been studied with regard to the response to successive small strain increments imposed on an initial relatively large strain deformation. For isotropic polymers, the results of such experiments have previously been interpreted in terms of a single thermally activated process modified by strain hardening. It has been found that, although this approach can describe satisfactorily some of the stress relaxation experiments on the oriented polyethylene fibres, it is unsatisfactory once the strain increments have exceeded a certain size, and that it is at variance with stress recovery experiments. It is shown that both the present stress relaxation and stress recovery experiments can be interpreted in terms of a model comprising two thermally activated processes acting in parallel. Furthermore, the parameters obtained for the stress relaxation data are consistent with those required to fit creep data obtained in a comparable stress range. The essential feature of the mechanical behaviour which was previously attributed to strain hardening can now be seen to arise from the transfer of stress between the two thermally activated processes in the two-process model.

1. Introduction

During the last few years, there have been several studies in this laboratory concerned with the creep and recovery behaviour of ultrahigh-modulus polyethylene fibres, instigated because of their potential load-bearing applications such as ropes and reinforcing fibres. It has been shown that the equilibrium creep behaviour can be described in terms of two thermally activated processes acting in parallel [1, 2], and this representation has been tentatively extended to deal with stress relaxation [3]. It has been recognized that this approach has kinship with that proposed by Escaig and his collaborators for the plastic deformation of isotropic glassy polymers such as polymethylmethacrylate and polystyrene [4, 5], and one of the authors (I.M.W.) is indebted to Professor Escaig for illuminating discussions at an early stage of the research at Leeds University.

The Escaig approach [4–7], which has been used to describe stress-relaxation behaviour, is, however, different in detail from that proposed by the Leeds group. Whereas the Leeds theory, as we shall term it, represents the behaviour by nonlinear viscoelasticity in terms of a pair of thermally activated Maxwell models in parallel, the Escaig theory consists of a single thermally activated Maxwell model together with a strain-hardening term. In this paper, we present experimental data on oriented polyethylene fibres. We show that, at least in this context, the Leeds model retains the desirable properties of the Escaig model, and also succeeds in modelling experimentally observed behaviour for oriented polyethylene fibres which is beyond the capability of the Escaig theory, while at the same time eliminating the need for the concept of strain-hardening.

1.1. The Escaig theory

The model consists of an elastic spring in series with a modified thermally activated dashpot, shown in Fig. 1. For a conventional Eyring thermally activated process [8], the plastic strain rate, $\dot{\varepsilon}_p$, corresponding to a stress, σ, is given by

$$\dot{\varepsilon}_p = \dot{\varepsilon}_{p0} \exp\left(\frac{-\Delta H}{kT}\right) \sinh\left(\frac{\sigma v}{kT}\right) \quad (1)$$

where $\dot{\varepsilon}_{p0}$ is the plastic strain rate corresponding to zero stress, ΔH the apparent activation enthalpy, k, Boltzmann's constant, T the temperature in degrees Kelvin, and v, the activation volume. For convenience this can be rewritten as

$$\dot{\varepsilon}_p = \dot{\varepsilon}'_{p0} \sinh(\sigma V) \quad (2)$$

where $\dot{\varepsilon}'_{p0} = \dot{\varepsilon}_{p0} \exp(-\Delta H/kT)$ and $V = v/kT$. For two states, 1 and 2, corresponding to non-zero stress

$$\dot{\varepsilon}_{p2} = \dot{\varepsilon}_{p1} \sinh(\sigma_2 V)/\sinh(\sigma_1 V) \quad (3)$$

and where $\sigma_1 V$ and $\sigma_2 V$ are suitably large

$$\dot{\varepsilon}_{p2} = \dot{\varepsilon}_{p1} \exp[(\sigma_2 - \sigma_1) V] \quad (4)$$

Escaig's modification of the thermally activated process is, in effect, to replace Equation 4 by

$$\dot{\varepsilon}_{p2} = \dot{\varepsilon}_{p1} \exp\{[\sigma_2 - \sigma_1 - K(\varepsilon_{p2} - \varepsilon_{p1})] V\} \quad (5)$$

where K is referred to as the strain hardening coefficient.

The motivation behind this modification originates from the results of experiments of the type illustrated in Fig. 2. A tensile specimen is rapidly loaded to a stress, $\sigma_0 + \Delta\sigma$, where $\Delta\sigma \ll \sigma_0$, and the strain then held constant while the stress is allowed to decay to the value σ_0, at which point the specimen is rapidly

0022–2461/90 $03.00 + .12

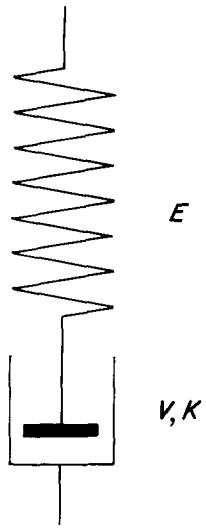

Figure 1 The Escaig model.

reloaded to the stress $\sigma_0 + \Delta\sigma$, and again allowed to relax, and so on. The time, Δt, for the stress to decay from $\sigma_0 + \Delta\sigma$ to σ_0 is observed at each step. It is reported that each successive decay time, Δt, exceeds the previous one by a constant factor; so that, for the ith and $(i + 1)$th loading step, the ratio of decay times $\Delta t_{i+1}/\Delta t_i$ exceeds unity and is constant independent of i. This behaviour is not consistent with Equations 3 or 4, because as there is no difference in stress between successive peaks (e.g. points A_1 and A_2 of Fig. 2), the plastic strain rate at such points would always be the same, so that each decay would be a copy of the previous one, implying that $\Delta t_{i+1}/\Delta t_i = 1$ for all i. However, it is readily shown that the predictions of the model of Fig. 1 when the dashpot is defined by Equation 5 conform with the reported behaviour.

The total strain, ε, is the sum of the elastic strain, ε_e, in the spring and the plastic strain, ε_p, in the dashpot, so that

$$\varepsilon = \varepsilon_e + \varepsilon_p \quad (6)$$

or

$$\varepsilon = \sigma/E + \varepsilon_p \quad (7)$$

where E is the modulus of the spring. Hence for a constant strain, ε

$$\dot{\varepsilon}_p = -\dot{\sigma}/E \quad (8)$$

and

$$\varepsilon_{p2} - \varepsilon_{p1} = -(\sigma_2 - \sigma_1)/E \quad (9)$$

where σ_1 and σ_2 are stresses at different times corresponding to plastic strains ε_{p1} and ε_{p2}.

Hence, Equations 8 and 9 can be used in Equation 5 to give a differential equation in stress corresponding to stress relaxation behaviour

$$\dot{\sigma}_2 = \dot{\sigma}_1 \exp[(1 + K/E)(\sigma_2 - \sigma_1) V] \quad (10)$$

This can be solved to give the stress at time t in terms of the stress at an earlier time zero

$$\sigma(t) = \sigma(0) - \ln(1 + t/c)/V(1 + K/E) \quad (11)$$

where

$$c = -[(1 + K/E)\dot{\sigma}(0)V]^{-1} \quad (12)$$

We associate zero time with the beginning of a decay cycle (points A_1 or A_2 in Fig. 2). For $K = 0$, Equation 11 is the Guiu and Pratt expression [9]. We can generate an expression involving Δt and $\Delta\sigma$ by making appropriate substitutions into Equation 11.

$$\Delta\sigma = \ln(1 + \Delta t/c)/V(1 + K/E)$$

from which we deduce that $\Delta t/c$ is constant, independent of the particular decay step. So for the ith and $(i + 1)$th cycles,

$$\begin{aligned}\Delta t_{i+1}/\Delta t_i &= c_{i+1}/c_i \\ &= \dot{\sigma}_i(0)/\dot{\sigma}_{i+1}(0) \quad \text{(using Equation 12)} \\ &= \dot{\varepsilon}_{pi}(0)/\dot{\varepsilon}_{pi+1}(0) \quad \text{(using Equation 8)} \\ &= \exp\{-K[\varepsilon_{pi}(0) - \varepsilon_{pi+1}(0)] V\} \\ &\quad \text{(using Equation 5)} \quad (13)\end{aligned}$$

If we assume that loading is so rapid that it results in no change in the plastic strain (i.e. that the plastic strain stays constant between points B_i and A_{i+1} in Fig. 2), then from Equation 7

$$\varepsilon_{pi+1}(0) - \varepsilon_{pi}(0) = \Delta\sigma/E$$

from which Equation 13 gives

$$\Delta t_{i+1}/\Delta t_i = \exp(KV\Delta\sigma/E) \quad (14)$$

The argument of the exponential is constant and positive, and so $\Delta t_{i+1}/\Delta t_i$ is constant and greater than 1. In

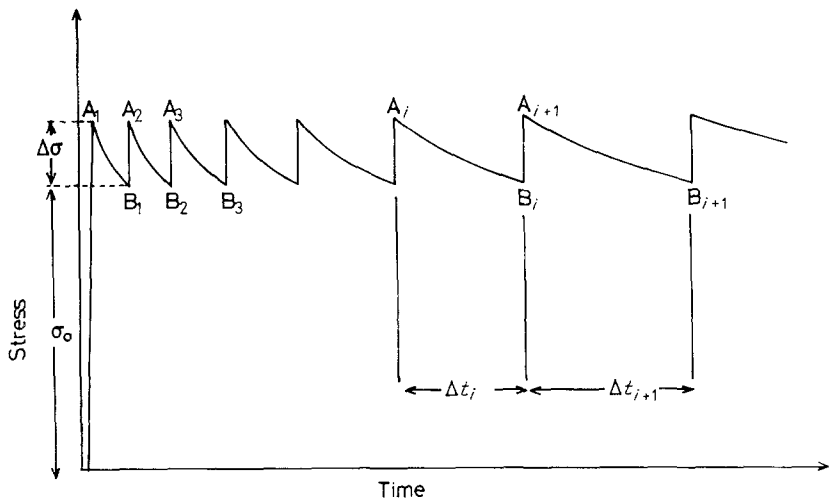

Figure 2 Step stress relaxation experiment.

this way the Escaig theory corresponds to experimental findings. Note that for $K = 0$, corresponding to the conventional Eyring process

$$\Delta t_{i+1} = \Delta t_i$$

Additional support for the Escaig theory derives from the fact that experimental relaxation curves are reported to fit very closely to Equation 11.

1.2. Critique of the Escaig theory and proposed alternative model

In the Escaig theory it is assumed that, in the experiment of Fig. 2, the increasing strain and the accompanying slowing down of the rate of stress decay are causally related. This is not the only possible interpretation; for instance, the slowing down of the stress decay rate might be an effect of a fading memory of the fast loading at the start of the experiment, and bear no relationship with the increasing strain. This question has led us to the consideration of the relaxation and recovery experiment illustrated schematically in Fig. 3, where the total strain decreases with time, as an experimental test of whether the causal relationship exists. In such an experiment, loading cycles resembling those of the original Fig. 2 experiment are followed by rapid partial unloading at time t_1 to a strain which is held constant, and the stress allowed to recover to a predetermined level at time t_3, and then unloaded to the same level as after the initial unloading, and further recovery allowed, and so on. Thus for times after t_2, the specimen strain now decreases at each unloading step, so that strain hardening events should be reversed, whereas the effects of any transients should continue to diminish as in the experiment of Fig. 2.

It is possible to set boundary conditions on the constant strain solution of Equation 11 which correspond to stress recovery (σ (0) > 0, $\dot{\sigma}$ (0) > 0) and then the equation yields recovery behaviour. As a result of the reversal of the strain hardening process, Equations 13 and 14 then operate so that the recovery times Δt_i and Δt_{i+1} for successive steps are implied to satisfy $\Delta t_i > \Delta t_{i+1}$. This speeding up of the stress recovery is both intuitively unlikely and in contradiction to our experimental observations, which give $\Delta t_i < \Delta t_{i+1}$. However, it is not truly a prediction of the Escaig theory, because the boundary condition $\dot{\sigma}$ (0) > 0 is not attainable by the model as a consequence of unloading. The Escaig model consists of elements in series, and so exhibits no recovery behaviour; after unloading, the stress continues to decay.

This in itself might be thought sufficient reason for the rejection of the theory for applications to polymers, which invariably show recovery behaviour. However, any model consisting of a small number of elements must be a simplification, because in reality a material would be equivalent to a complex array of many elements. Transfer of stress from networks which are in tension to parallel networks which are in compression can be assumed to be the source of recovery behaviour. The Escaig model could therefore be oversimplified in a way which makes it inadequate for representing recovery behaviour, and yet still retain some basic validity. A way to examine this possibility would be to propose a more complex model with some capability of stress recovery; the obvious such model consists of two Escaig models with unequal parameters in parallel. However, we shall show that this model is actually more complex than is necessary, because, once the need for a parallel network is accepted, all the observed experimental behaviour can be accounted for without the need for the introduction of strain hardening coefficients.

Consider the model of Fig. 4, consisting of springs with stiffness E^a and E^b with $E^a > E^b$ and Eyring dashpots characterized by V^a and V^b, $\dot{\varepsilon}^a_{p0}$ and $\dot{\varepsilon}^b_{p0}$. This model, termed the two-process model, has been applied previously to creep [1, 2] and to single-step stress relaxation [1]. A schematic diagram of its response to the experimental regime of Fig. 2 is shown in Fig. 5, in which the stress in the model is decomposed into the stress in the a-arm and the stress in the b-arm. If the properties of the two arms differ appreciably, it is inevitable that one will undergo a net loss in stress, and the other a corresponding net gain, with each decay cycle (e.g. between points A_i and A_{i+1}). If the a-arm, which already holds most of the stress, acquires more, then within a few cycles it will hold almost all of the stress, and the system will behave as a single process model. If, however, the b-process gains in stress as illustrated, a more interesting system results in which the process of transfer of stress between the two arms can last for many cycles. Moreover, the decay time, Δt_i, will increase at each step. This

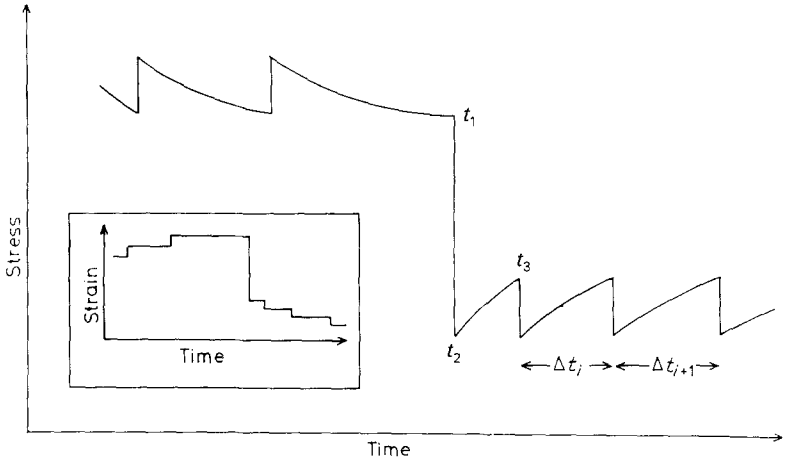

Figure 3 Stress relaxation and recovery experiment.

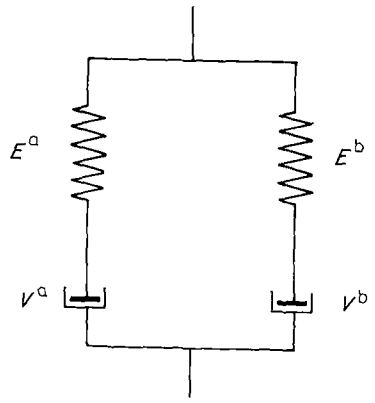

Figure 4 The two-process (Leeds) model.

becomes apparent when we note that, at least in the initial stages, the a-process has the faster decay rate and is therefore the dominant factor in determining Δt_i; and that at each step, some stress leaks from the a-process to the b-process, so that the plastic strain rate $|\dot{\varepsilon}_p^a|$ falls at successive peaks (see Equation 3), with the result that the rate of stress decay $|\dot{\sigma}^a| = E^a|\dot{\varepsilon}_p^a|$ (adapting Equation 8) also decreases, and that finally Δt_i increases. It is also clear that this process of stress transfer will eventually cease when the stress in each arm reaches a level at which there is no net change at successive peaks, when $\Delta t_{i+1} = \Delta t_i$. At this stage it is not obvious whether this is an important characteristic of the model, because this steady state might not be reached within experimental time scales. We also note that for recovery behaviour the model returns the correct response $\Delta t_{i+1} \geqslant \Delta t_i$ for successive recovery times; with one arm in tension and the other in compression, the stress in each arm decreases in absolute value during recovery, and so the stress decay rate in each arm, and therefore in the total system, decreases.

We now show that the two-process model's predictions of the stress for the experiment of Fig. 2 are consistent with $\Delta t_{i+1}/\Delta t_i \simeq$ constant for some range of experimental time. For this analytical argument we use the exponential approximation to the Eyring process of Equation 4, whereas for quantitative calculations in succeeding sections we shall use numerical methods and the exact hyperbolic sine function of Equations 2 and 3. Suppose a particular decay cycle begins at time t_A and ends at t_B, corresponding to points A_i and B_i in Fig. 5. Then, adapting Equations 8 and 11 with $K = 0$

$$\sigma_A^a - \sigma_B^a = \ln [1 + (t_B - t_A)V^a E^a \dot{\varepsilon}_{pA}^a]/V^a \quad (15)$$

for the a-arm and

$$\sigma_A^b - \sigma_B^b = \ln [1 + (t_B - t_A)V^b E^b \dot{\varepsilon}_{pA}^b]/V^b \quad (16)$$

for the b-arm, where it is understood that subscripts A or B refer to values at times t_A and t_B.

Adding the above two equations and writing $t_B - t_A = \Delta t$ gives

$$\Delta\sigma = \ln [(1 + \Delta t V^a E^a \dot{\varepsilon}_{pA}^a)^{1/V^a} \times (1 + \Delta t V^b E^b \dot{\varepsilon}_{pA}^b)^{1/V^b}] \quad (17)$$

This is true for any cycle. Equating arguments on the right-hand side for successive ith and $(i + 1)$th cycles gives

$$(1 + \Delta t_i V^a E^a \dot{\varepsilon}_{pAi}^a)(1 + \Delta t_i V^b E^b \dot{\varepsilon}_{pAi}^b)^{V^a/V^b} = (1 + \Delta t_{i+1} V^a E^a \dot{\varepsilon}_{pAi+1}^a)(1 + \Delta t_{i+1} V^b E^b \dot{\varepsilon}_{pAi+1}^b)^{V^a/V^b} \quad (18)$$

It will be shown below that for physically relevant values of the parameters

$$\Delta t_i V^a E^a \dot{\varepsilon}_{pAi}^a \ll 1 \quad (19)$$

and that the other three similar quantities in Equation 18 share this property. Equating first-order terms in Equation 18 now gives

$$\Delta t_i V^a (E^a \dot{\varepsilon}_{pAi}^a + E^b \dot{\varepsilon}_{pAi}^b) = \Delta t_{i+1} V^a \times (E^a \dot{\varepsilon}_{pAi+1}^a + E^b \dot{\varepsilon}_{pAi+1}^b)$$

By assumption, $E^a > E^b$, and so after the initial rapid loading step $\sigma^a > \sigma^b$. Subsequently, provided that V^a does not differ too greatly from V^b and $\dot{\varepsilon}_{p0}^a$ does not differ too greatly from $\dot{\varepsilon}_{p0}^b$, by Equation 2 $\dot{\varepsilon}_{pAi}^a > \dot{\varepsilon}_{pAi}^b$. It is thus possible that the values of the various parameters can be such that the second terms in parentheses on either side of Equation 19 may be neglected. Then, to first order $\Delta t_i \dot{\varepsilon}_{pAi}$ is independent of i, hence

$$\Delta t_i \dot{\varepsilon}_{pAi} \simeq \text{constant} \quad (20)$$

It then follows from Equation 15 that $\sigma_{Ai}^a - \sigma_{Bi}^a$ is independent of i. If we assume that loading between times t_{Bi} and t_{Ai+1} is so fast that only the springs are extended, then the difference between stresses at

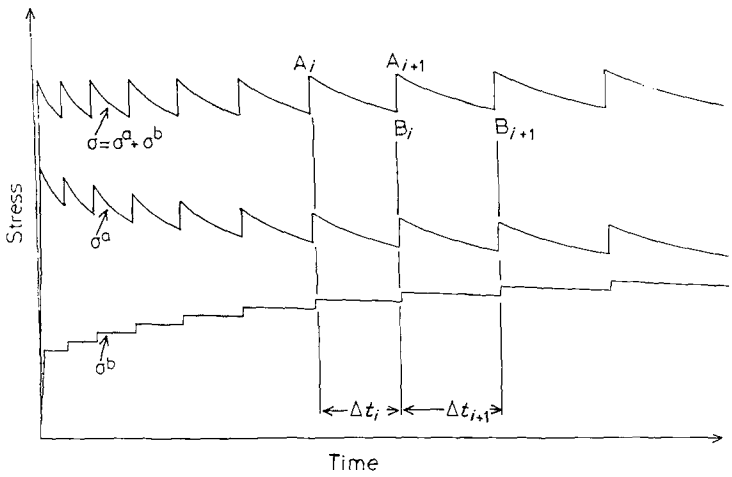

Figure 5 Decomposition of stress in Leeds model representation of step stress relaxation experiment.

successive peaks is given by

$$\sigma^{a}_{Ai+1} - \sigma^{a}_{Ai} = \sigma^{a}_{Bi} + \Delta\sigma E^{a}/(E^{a} + E^{b}) - \sigma^{a}_{Ai}$$

which is again a constant. The ratio of plastic strain rates at successive peaks is now given by Equation 4 as the constant

$$\dot{\varepsilon}^{a}_{pAi+1}/\dot{\varepsilon}^{a}_{pAi} = \exp[(\sigma^{a}_{Ai+1} - \sigma^{a}_{Ai})V^{a}]$$

so that from Equation 20 we have

$$\Delta t_{i+1}/\Delta t_{i} \simeq \exp[(\sigma^{a}_{Ai} - \sigma^{a}_{Ai+1})V^{a}) \qquad (21)$$

which, because the stress in the a-process is falling, is a constant greater than one. Equation 21 shows that the two-process model can give predictions which resemble those of the Escaig theory. The equation will cease to describe the model behaviour after a finite number of cycles, and this number will depend on the particular values of the model parameters. The ability of this, the Leeds model, to represent experimentally observed behaviour in detail will now be examined.

2. Experimental details

The performance of step stress relaxation of the type shown in Fig. 2 presents problems both of control (the stopping or starting of rapid straining in response to the force signal) and of data handling, due to the large amount of data generated. These problems are solved by the use of microcomputers in the experimental set-up illustrated in Fig. 6. Strain is applied to the specimen by an electric motor operating via a gear box, controlled by an electromagnetic clutch, and the force in the specimen sensed by a strain gauge transducer. The motor and clutch are controlled by digital signals from a EUROBEEB single board microcomputer which operates together with a Cumen-Selecta sideways memory carrier and a CUBAN twelve-bit analogue interface (Control Universal Ltd, Cambridge, UK). The force signal, in the form of the analogue output from the strain gauge conditioner unit, is read by this ensemble. A program written in REAL TIME BASIC running on the EUROBEEB controls the switching of the motor and clutch and the times at which the force is read, and stores force readings and their times in RAM. Because of the slow speed of analogue to digital conversion, the analogue force signal is not used as a basis for the control of motor and clutch; rather, two digital signals are generated for this purpose by comparator circuits, with the senses of the signals depending on whether the force signal exceeds or is less than two levels preset by potentiometers. The screen, keyboard and disc drives of a BBC Master 128 microcomputer (Acorn Computers Ltd, Cambridge, UK) serve the EUROBEEB. Programs run on the Master 128 allow for data transfer from the EUROBEEB on to floppy disk. Data can be retrieved from disk and displayed and analysed during the course of the experiments.

The material used was a multifilament polyethylene fibre, prepared by melt-spinning and drawing to a ratio 30 (Alathon 7050, Celanese Fibers Company, North Carolina, USA). Fibre specimens of length 65 mm and cross-section 0.33 mm^2 were subjected to step stress relaxation tests, with lower limit stress $\sigma_0 = 205$ MPa, and $\Delta\sigma$ varying between experiments from $\Delta\sigma = 13.7$ to 58.4 MPa. The fast loading was at a strain rate of 1.2×10^{-3} sec^{-1}.

2.1. Application of the two-process model

In addition to the stress relaxation data obtained in the experiments described so far, creep data for this material are available and have been reported in a previous publication [2]. Because a valid theory of nonlinear viscoelasticity should be capable of modelling all mechanical behaviour, we apply the two-process model to both the creep data and the stress relaxation data, using the same values for the model parameters. These values have been obtained by a process of trial and error, and we make no claim for their uniqueness.

Initial estimates of the values of V^{a}, V^{b}, $\dot{\varepsilon}^{a}_{0}$ and $\dot{\varepsilon}^{b}_{0}$ were made on the basis of the observed equilibrium creep rates, which are functions of these parameters only. It was then necessary to determine whether such estimates were consistent with the transient creep and stress relaxation behaviour, and to manipulate the values of E^{a} and E^{b} to obtain the best possible fit with the non-equilibrium experimental data.

2.2. Stress relaxation: decay time ratios

We implement the two-process model by solving numerically the Eyring Equation 3 for the stress at constant rate of strain for each arm of the model; the total stress is then the sum of the stresses in the two arms.

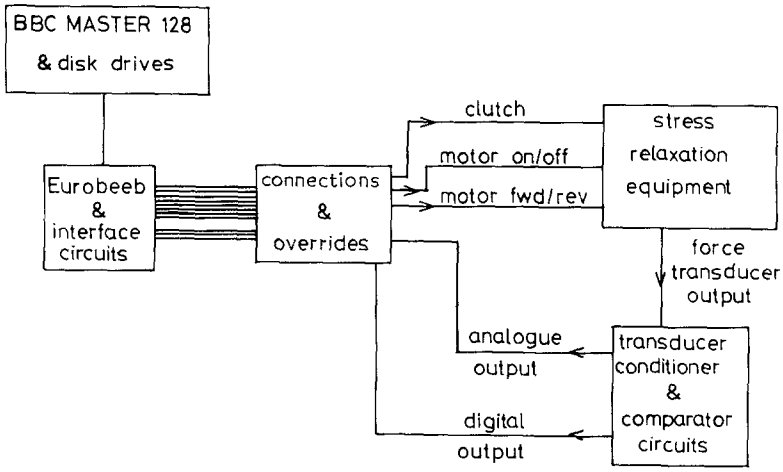

Figure 6 Block diagram of experimental, control and data acquisition equipment for stress relaxation experiments.

Rewriting Equation 3 for the a-arm gives

$$\dot{\varepsilon}^{a}_{p2} = \dot{\varepsilon}^{a}_{p1} \sinh(\sigma^{a}_{2}V^{a})/\sinh(\sigma^{a}_{1}V^{a}) \quad (22)$$

and for a strain rate $\dot{\varepsilon}$ we have

$$\dot{\varepsilon}^{a}_{p} + \dot{\sigma}^{a}/E^{a} = \dot{\varepsilon} \quad (23)$$

These equations, and similar equations for the b-process, can be solved by a finite difference method when σ^{a}_{1} and σ^{a}_{2} denote stresses at times separated by a short time increment and $\dot{\varepsilon}$ is assumed to be constant. Details of the solution are given in the Appendix. The same subroutine is used for both the loading and the relaxing stress calculations, with the strain rate assigned the value zero in the latter case. The process is begun from zero stress using a similar routine in which Equation 2 is used rather than Equation 3.

During this experiment, various imperfections ensure that the stress increment, $\Delta\sigma$, is not exactly the same at each step. To avoid unnecessary error in the predictions, we base them on the stress increment actually observed rather than relying on a constant average value. Predictions and experimental results are compared in Figs 7 to 12, where $\Delta t_{i+1}/\Delta t_i$ is plotted against the cycle number, i. The model parameters used for these calculations are listed in Table I. The figures show results for $\sigma_0 = 205$ MPa and average values of $\Delta\sigma$ of 13.7, 29.8, 36.9, 46.2, 52.3 and 58.4 MPa, respectively, in Figs 7, 8, 9, 10, 11, and 12. Fig. 7 shows an apparently constant $\Delta t_{i+1}/\Delta t_i$ over 32 decay cycles; this is precisely the behaviour which is cited as support for the Escaig model, but it is clear that the two-process model also conforms to the experimental behaviour. The prediction of the total time elapsed during this experiment is in good agreement with that observed. All the subsequent figures show $\Delta t_{i+1}/\Delta t_i$ to be decreasing with increasing i, and the model predictions also conform with this. We have already noted that the model should begin to behave in this way as the process of transfer of stress from one arm to the other nears completion. The prediction of this effect is beyond the capability of the Escaig model, for which $\Delta t_{i+1}/\Delta t_i$ is constant. The observed increase in the initial values of $\Delta t_{i+1}/\Delta t_i$ as $\Delta\sigma$ is increased is also predicted by the two-process model. It is apparent, however, that the quality of the predictions of the two process model deteriorate as $\Delta\sigma$ is increased.

2.3. Stress relaxation: relaxation curves

According to the model results of the previous section, for all the experiments, $\dot{\sigma}^{a} \gg \dot{\sigma}^{b}$ at all times. The difference is greatest for the earliest cycle numbers, where it is many orders of magnitude, and is never less

TABLE I Fitting parameters for stress relaxation $\sigma_0 =$ 205 MPa, creep $\sigma_0 =$ 150, 190 and 280 MPa

	a	b
V (GPa)$^{-1}$	64*	44†
E (GPa)	28	2.5
$\dot{\varepsilon}'_0$ (sec^{-1})	4.1×10^{-8}	3.2×10^{-7}

*$v \simeq 260 \times 10^{-30}$ m^3.
†$v \simeq 180 \times 10^{-30}$ m^3.

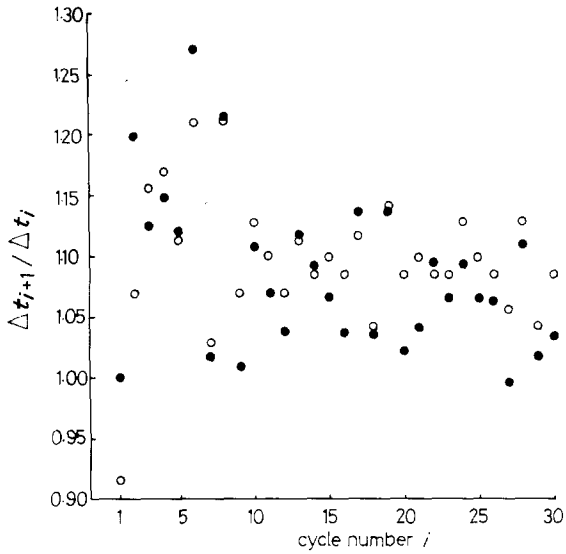

Figure 7 Decay time ratios for step stress relaxation with $\sigma_0 =$ 205 MPa and $\Delta\sigma = 13.7$ MPa; (●) observed, (○) predicted.

than a factor of ten. It follows that, for the total stress σ, $\dot{\sigma} = \dot{\sigma}^{a} + \dot{\sigma}^{b} \simeq \dot{\sigma}^{a}$, and for the stresses at times t_1 and t_2, $\sigma_2 - \sigma_1 \simeq \sigma^{a}_{2} - \sigma^{a}_{1}$. Using the exponential approximation for the a-arm (adapting Equation 10 with $K = 0$) gives

$$\dot{\sigma}^{a}_{2} = \dot{\sigma}^{a}_{1} \exp[(\sigma^{a}_{2} - \sigma^{a}_{1})V^{a}]$$

which in the light of the above approximations is equivalent to

$$\dot{\sigma}_2 = \dot{\sigma}_1 \exp[(\sigma_2 - \sigma_1)V^{a}]$$

and we know (see Equations 11 and 12 that this equation has the Guiu and Pratt [9] solution

$$\sigma(t) = \sigma(0) - \ln(1 + t/c)/V^{a} \quad (24)$$

where $c = -[\dot{\sigma}(0)V^{a}]^{-1}$. Thus, in this case, the Leeds model gives the same form of equation for the relaxation curves as does the Escaig model. A further implication is that the relaxation curves for the experiments of Figs 7 to 12 should fit Equation 24, and that such fitting should yield values of V^{a} consistent with the value assumed and given in Table I.

All the stress relaxation curves of the experiments of Figs 7 to 12 were fitted to Equation 24 using a least squares routine which operated by iterating the parameter c. The routine was implemented by a program running on the BBC Master 128 using the experimental data stored on floppy disks. Equation 24 was

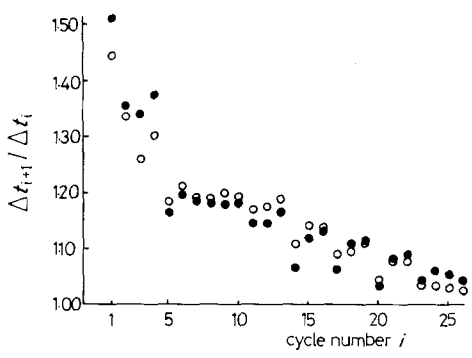

Figure 8 Decay time ratios for step stress relaxation with $\sigma_0 =$ 205 MPa and $\Delta\sigma = 29.8$ MPa; (●) observed, (○) predicted.

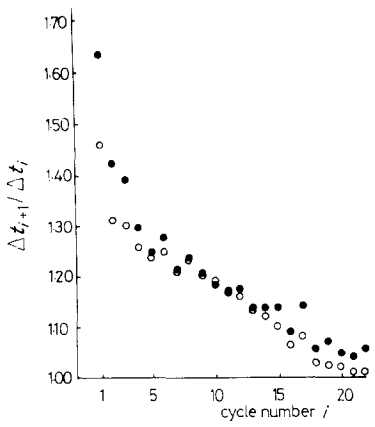

Figure 9 Decay time ratios for step stress relaxation with σ_0 = 205 MPa and $\Delta\sigma$ = 36.9 MPa; (●) observed, (○) predicted.

found to fit all the curves very well. Values of V^a were thus obtained for each curve, and are plotted in Fig. 13 as a function of σ^a. The values cluster around the assumed value of 64 GPa^{-1}, but with a trend of V^a decreasing with increasing σ^a. If this is not due to systematic error, it may indicate that the assumed constant value of V^a is a first approximation and the derived values a more refined approximation; but whether this behaviour would be due to a true dependence of V^a on σ^a, or to a stress transfer process between elements of an array of greater complexity than that assumed in the Leeds theory, is a question that cannot be addressed at this stage.

2.4. Creep

To calculate creep rates from the two-process model we first use Equations 22 and 23 to derive an expression for strain rate

$$\dot{\varepsilon}_2 = \dot{\varepsilon}^a_{p1} \sinh(\sigma^a_2 V^a)/\sinh(\sigma^a_1 V^a) + \dot{\sigma}^a_2/E^a \tag{25}$$

For creep, $\sigma = \sigma^a + \sigma^b$ and $\dot{\sigma} = \dot{\sigma}^a + \dot{\sigma}^b = 0$. The analogue of Equation 25 for the b-arm then becomes

$$\dot{\varepsilon}_2 = \dot{\varepsilon}^b_{p1} \sinh[(\sigma - \sigma^a_2)V^b]/\sinh[(\sigma - \sigma^a_1)V^b] - \dot{\sigma}^a_2/E^b \tag{26}$$

Subtracting Equations 26 from 25 gives a differential

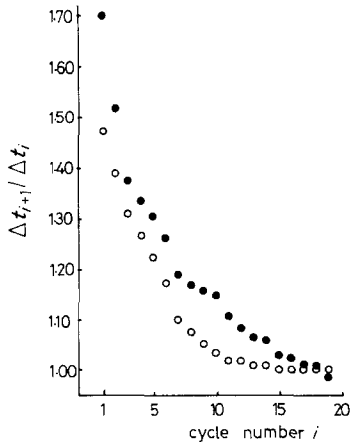

Figure 10 Decay time ratios for step stress relaxation with σ_0 = 205 MPa and $\Delta\sigma$ = 46.2 MPa; (●) observed, (○) predicted.

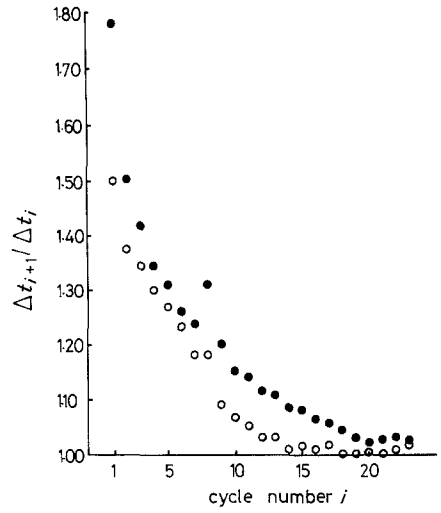

Figure 11 Decay time ratios for step stress relaxation with σ_0 = 205 MPa and $\Delta\sigma$ = 52.3 MPa; (●) observed, (○) predicted.

equation in σ^a_1 and σ^a_2

$$\dot{\varepsilon}^a_{p1} \sinh(\sigma^a_2 V^a)/\sinh(\sigma^a_1 V^a) - \dot{\varepsilon}^b_{p1} \sinh[(\sigma - \sigma^a_2)V^b]/\sinh[(\sigma - \sigma^a_1)V^b] + \dot{\sigma}^a_2(1/E^a + 1/E^b) = 0 \tag{27}$$

which can be solved by finite differences when σ^a_1 and σ^a_2 correspond to times separated by a small time increment. The details of this calculation are given in the Appendix. Once σ^a_1 and σ^a_2 are known, the strain rate can be calculated from Equation 25. The stress is assumed to be initially applied to the specimen at a high rate of strain, and the same calculation method is used as for the stress relaxation work.

In Fig. 14 we compare observed and predicted creep rates for stresses of 150, 190 and 280 MPa, in the form of strain rate against strain (Sherby–Dorn [10]) plots. The calculations were performed using the values of the parameters listed in Table I. The initial loading was assumed to be at a strain rate of 10^{-2} sec^{-1} corresponding to loading times of 0.5 to 3 sec, and it was

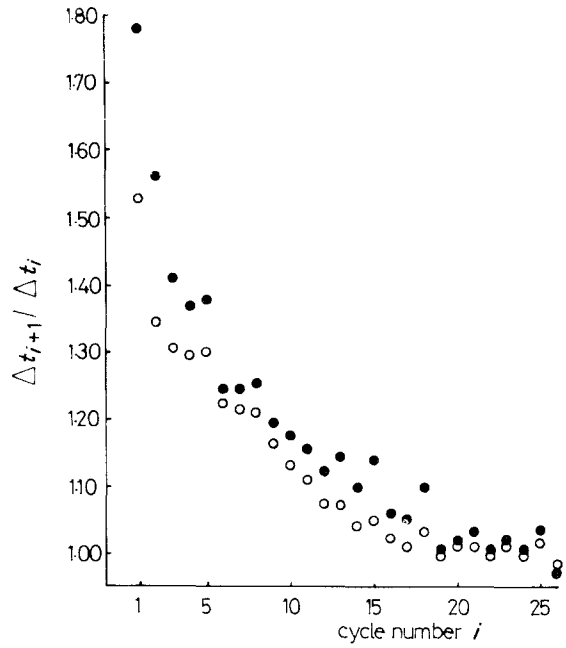

Figure 12 Decay time ratios for step stress relaxation with σ_0 = 205 MPa and $\Delta\sigma$ = 58.4 MPa; (●) observed, (○) predicted.

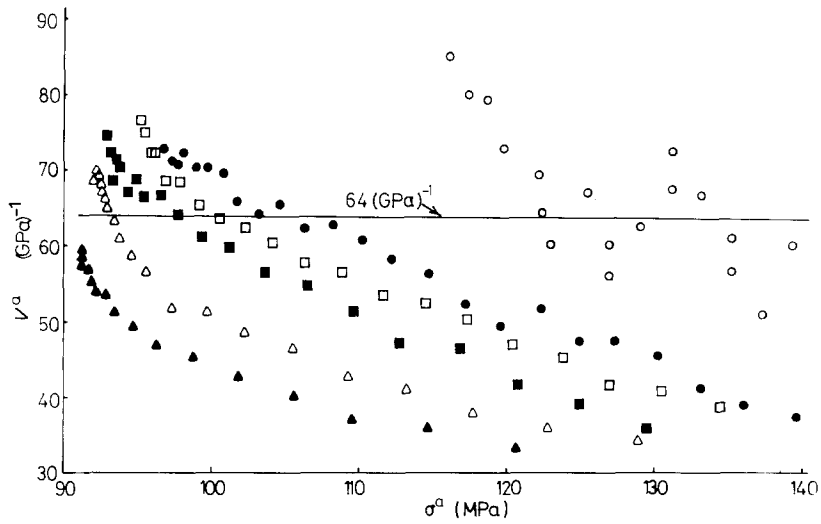

Figure 13 Values of V^a derived from the relaxation curve fits on the experiments of Figs 7 to 12. $\Delta\sigma$ values: (○) 13.7, (●) 29.8, (□) 36.9, (■) 46.2, (△) 52.3 and (▲) 58.4 MPa.

verified that substituting a strain rate of 10^{-1} sec^{-1} had a negligible effect. The calculated strain rates are close to the observed ones except at short times.

3. Discussion and conclusions

The evidence presented has shown that the two-process model gives a consistent representation of creep and stress relaxation for stresses in the range 150 to 280 MPa, and that the Escaig theory cannot conform to the observed phenomena. The desirable properties of the Escaig theory – the increasing decay time in step stress relaxation experiments, and the predicted shape of relaxation curves – are shared by the Leeds theory. Further experiments have shown that the Leeds model, when used with the data of Table I, does not give valid predictions at stresses much below the stated range; the modelled creep behaviour at 110 MPa is seriously in error, as are predictions of step stress relaxation for $\sigma_0 \simeq 100$ MPa. However, predictions of similar quality to the ones discussed in the previous section, for a similar exercise involving stress relaxation with $\sigma_0 = 100$ MPa and a range of values of $\Delta\sigma$ and also for creep at 110 MPa, were obtained with the data of Table II. The need for stress dependent parameters indicates that the two process model is an oversimplification. We can conclude that, while the Leeds model may not give a true representation of events in detail, the type of stress transfer process which it embodies is at the root of observed viscoelastic behaviour.

As an example of a stress transfer process in a more complex model, we can envisage a large parallel network of thermally activated Maxwell models with differing properties; during stress relaxation or creep, some of the Maxwell models gain stress at the expense of others which lose stress, and the two-process Leeds model would approximate to this by lumping together the stress-gaining Maxwell models as one arm and the stress-losing models as the other arm. The relative populations of the stress-gaining and stress-losing Maxwell models, and therefore the values of the parameters in the approximating Leeds model, would depend on the applied stress.

Values for the parameters of the two-process model have been reported previously [2] which were based on the equilibrium creep rates and yield behaviour of the material studied here. These values were calculated on the assumption that the parameters were constant in the range 110 to 900 MPa, the derived activation volumes, v, for the two processes being 327×10^{-30} and 30.7×10^{-30} m^3 (corresponding to values of V of 81 and 7.6 GPa^{-1}). According to the model predictions, the smaller activation volume was dominant at high stresses, whereas below 300 MPa the larger activation volume was dominant, accounting for 99.8%, 90% and 69% of the total stress at 110, 190 and 280 MPa respectively. The present results are relevant to this lower stress range, and it is significant that the values $V^a = 64$ GPa^{-1} and $V^a = 100$ GPa^{-1} of Tables I and II do not severely conflict with the

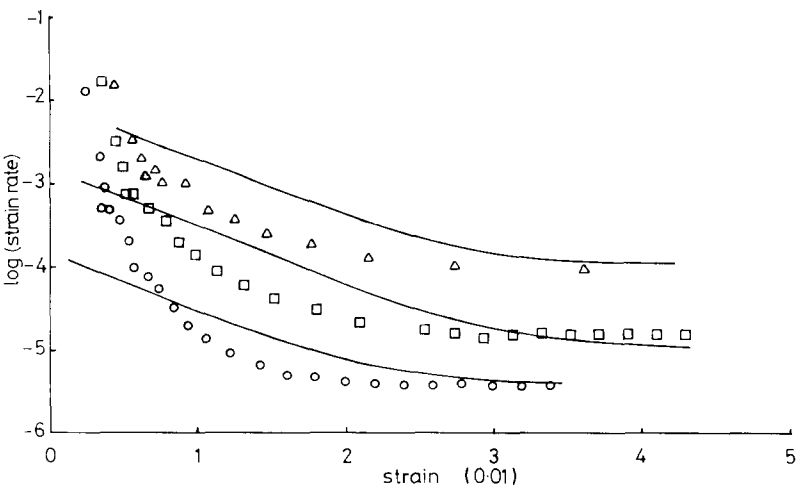

Figure 14 Observed creep rates at (○) 150, (□) 190 and (△) 280 MPa, together with Leeds model predictions represented by lines.

TABLE I Fitting parameters for stress relaxation σ_0 = 205 MPa, creep σ_0 = 150, 190 and 280 MPa

	a	b
V (GPa)$^{-1}$	64*	44†
E (GPa)	28	2.5
$\dot{\varepsilon}'$(sec^{-1})	4.1×10^{-8}	3.2×10^{-7}

*$v \simeq 260 \times 10^{-30}$ m^3.
†$v \simeq 180 \times 10^{-30}$ m^3.

value $V = 81\,\text{GPa}^{-1}$ derived from the constant-parameter fit and associated with the process which is calculated to be dominant in this stress range. Our present detailed study has shown that the assumption of constant (i.e. stress-independent) parameters is incorrect, but a fitting procedure derived on this basis would be expected to yield approximate data for the dominant process. We can apply similar reasoning for the higher (up to 900 MPa) stress range where the smaller activation volume is calculated to be dominant, and would expect that the value obtained for this activation volume to be physically significant in the high-stress regime. This activation volume has been identified with the α-relaxation process, which is widely believed to be associated with crystalline c-slip in terms of a Reneker-like defect moving through the crystalline regions.

Appendix: Numerical solutions of equations of the two-process model

A.1. Step stress relaxation experiments

The stress relaxation experiments are programmes consisting of regimes of both constant strain rate loading and of stress relaxation at constant strain. In either case the strain rate is constant, and the same numerical routine is used to calculate the stress. The governing Equations are 21 and 22. Subscripts i-1 and i refer to states separated by a time increment Δt. A finite difference formulation is used, using forward differences, so that the time derivative of stress in the a-arm is approximated by assuming that

$$\dot{\sigma}_i^a = (\sigma_i^a - \sigma_{i-1}^a)/\Delta t \quad \text{(A1)}$$

Using Equation 21 this becomes

$$\dot{\sigma}_i^a = (\sinh^{-1}[(\dot{\varepsilon}_{pi}^a/\dot{\varepsilon}_{pi-1}^a) \sinh (\sigma_{i-1}^a V^a)]/V^a - \sigma_{i-1}^a)/\Delta t \quad \text{(A2)}$$

Then using Equation 22

$$\dot{\varepsilon}_{pi}^a + (\sinh^{-1}[(\dot{\varepsilon}_{pi}^a/\dot{\varepsilon}_{pi-1}^a) \times \sinh (\sigma_{i-1}^a V^a)]/V^a - \sigma_{i-1}^a)/E^a \Delta t - \dot{\varepsilon} = 0 \quad \text{(A3)}$$

where $\dot{\varepsilon}$ is the constant strain rate. At each time increment Equation A3 is solved for $\dot{\varepsilon}_{pi}^a$ using Newton's method [11]. The stress σ_i^a is then given by the relation

$$\sigma_i^a = \sinh^{-1}[\dot{\varepsilon}_{pi} \sinh (\sigma_{i-1}^a V^a)/\dot{\varepsilon}_{pi-1}]$$

obtained by rearranging Equation 21. The same method is used to obtain σ_i^b, and thus the total stress $\sigma_i = \sigma_i^a + \sigma_i^b$. The value of σ_i determines whether or not the value of strain rate used for the calculation for the next time step is changed, from the rapid loading value to zero when $\sigma_i > \sigma_0 + \Delta\sigma$, or from zero to the rapid loading value when $\sigma_i < \sigma_0$. Different values of Δt are used for the rapid loading and stress relaxation regimes.

The process starts with $\sigma_{i-1}^a = \sigma_{i-1}^b = 0$, and so for the first time increment Equation A2 is replaced by an equation based on Equation 2 rather than Equation 21, with the result that Equation A3 is replaced by

$$\dot{\varepsilon}_{p1}^a + \sinh^{-1}(\dot{\varepsilon}_{p1}^a/\dot{\varepsilon}_{p0}^a)/V^a E^a \Delta t - \dot{\varepsilon} = 0$$

which is also solved by Newton's method.

A.2. Creep experiments

Here the governing equation is Equation 26. The forward difference method is again used and we obtain for a constant total stress, σ

$$\dot{\varepsilon}_{pi-1}^a \sinh (\sigma_i^a V^a)/\sinh (\sigma_{i-1}^a V^a) - \dot{\varepsilon}_{pi-1}^b \sinh [(\sigma - \sigma_i^a)V^b]/\sinh [(\sigma - \sigma_{i-1}^a)V^b] + (\sigma_i^a - \sigma_{i-1}^a)(1/E^a + 1/E^b)/\Delta t = 0 \quad \text{(A4)}$$

Equation A4 is solved by Newton's method for σ_i^a. The total creep rate $\dot{\varepsilon}_i$ is then given by Equation 24

$$\dot{\varepsilon}_i = \dot{\varepsilon}_{pi-1}^a \sinh (\sigma_i^a V^a)/\sinh (\sigma_{i-1}^a V^a) + (\sigma_i^a - \sigma_{i-1}^a)/E^a \Delta t$$

The initial loading to the constant stress, σ, is assumed to be at a constant strain rate, and the routines used for the stress relaxation calculations are employed to give the values of σ_{i-1}^a, σ_{i-1}^b, $\dot{\varepsilon}_{pi-1}^a$, $\dot{\varepsilon}_{pi-1}^b$ corresponding to the initial loading.

Acknowledgement

We wish to thank Dr G. R. Davies for invaluable assistance in the development of the experimental computer control and data handling and processing.

References

1. M. A. WILDING and I. M. WARD, *Polymer* **22** (1981) 871.
2. P. G. KLEIN, D. W. WOODS and I. M. WARD, *J. Polym. Sci. Polym. Phys. Edn* **25** (1987) 1359.
3. M. A. WILDING and I. M. WARD, *J. Mater. Sci.* **19** (1984) 629.
4. J. P. CAVROT, J. HAUSSY, J. M. LEFEBVRE and B. ESCAIG, *Mater. Sci. Engng* **36** (1978) 95.
5. J. HAUSSY, J. P. CAVROT, B. ESCAIG and J. M. LEFEBVRE, *J. Polym. Sci. Polym. Phys. Edn* **18** (1980) 311.
6. B. ESCAIG, in "Plastic Deformation of Amorphous and Semi-Crystalline Materials", edited by B. Escaig and C. G'Sell (Les Editions de Physique, Les Ulis, 1982) p. 187.
7. J. M. LEFEBVRE and B. ESCAIG, *J. Mater. Sci.* **20** (1985) 438.
8. H. EYRING, *J. Chem. Phys.* **4** (1936) 283.
9. F. GUIU and P. L. PRATT, *Phys. Status Solidi* **6** (1964) 111.
10. O. D. SHERBY and J. E. DORN, *J. Mech. Phys. Solids.* **6** (1956) 145.
11. C. F. GERALD, "Applied Numerical Analysis" (Addison Wesley, London, 1978).

Received 28 October 1988
and accepted 14 April 1989